Multiscale Characterization and Model for the Dynamic Behavior of Ferroelectric Materials Using Fractional Operators

Benjamin Ducharne, Grzegorz Litak, Bin Zhang, Bhaawan Gupta

▶ **To cite this version:**

Benjamin Ducharne, Grzegorz Litak, Bin Zhang, Bhaawan Gupta. Multiscale Characterization and Model for the Dynamic Behavior of Ferroelectric Materials Using Fractional Operators. Kenan Taş; Dumitru Baleanu; J. A. Tenreiro Machado. Mathematical Methods in Engineering. Applications in Dynamics of Complex Systems, 24, Springer, pp.139-152, 2019, Nonlinear Systems and Complexity, 978-3-319-90971-4. 10.1007/978-3-319-90972-1_10 . hal-02051553

HAL Id: hal-02051553
https://hal.science/hal-02051553

Submitted on 13 Apr 2022

HAL is a multi-disciplinary open access archive for the deposit and dissemination of scientific research documents, whether they are published or not. The documents may come from teaching and research institutions in France or abroad, or from public or private research centers.

L'archive ouverte pluridisciplinaire **HAL**, est destinée au dépôt et à la diffusion de documents scientifiques de niveau recherche, publiés ou non, émanant des établissements d'enseignement et de recherche français ou étrangers, des laboratoires publics ou privés.

Distributed under a Creative Commons Attribution - NonCommercial 4.0 International License

Multiscale Characterization and Model for the Dynamic Behavior of Ferroelectric Materials Using Fractional Operators

Benjamin Ducharne, Grzegorz Litak, Bin Zhang, and Bhaawan Gupta

10.1 Introduction

Ferroelectric and piezoelectric materials are widely used in many areas of technology and science. The sensors based on the piezoelectric effect transform mechanical signals into electrical signals and are used as accelerometers or for pressure and vibration measurements [1–3]. Except in memory applications, which are based on polarization switching and hysteresis polarization-electric field relationships, hysteresis is undesired in high-precision sensor, actuator, and capacitor applications. Origins and mechanisms of the piezoelectric hysteresis are complex, and they manifest themselves in qualitatively different forms. An ideal hysteresis loop is

B. Ducharne
Laboratoire de Genie Electrique et Ferroelectricite, Institut National des Sciences Appliquees de Lyon, Villeurbanne, France
e-mail: benjamin.ducharne@insa-lyon.fr

G. Litak
Laboratoire de Genie Electrique et Ferroelectricite, Institut National des Sciences Appliquees de Lyon, Villeurbanne, France

Faculty of Mechanical Engineering, Lublin University of Technology, Lublin, Poland

Department of Process Control, AGH University of Science and Technology, Kraków, Poland
e-mail: g.litak@pollub.pl

B. Zhang
Reseach Center of Mechanics and Mechatronic Equipment, Shandong University, Weihai, China
e-mail: bin.zhang@sdu.edu.cn

B. Gupta
Laboratoire de Genie Electrique et Ferroelectricite, Institut National des Sciences Appliquees de Lyon, Villeurbanne, France

ELYTLAB, TOHOKU University, Sendaï, Japan
e-mail: bhaawan.gupta@insa-lyon.fr

symmetrical, so the absolute value of the positive and negative coercive fields and positive and negative remnant polarizations is equal [4, 5]. Hysteresis loops are highly frequency dependent. The main consequences of a frequency increase on hysteresis loops are:

– Increasing coercive fields.
– Decreasing remnant polarizations.
– Varying hysteresis loop areas [6–8].

Fractional operators are particularly well adapted to model the frequency dependence of the dielectric hysteresis of a ferroelectric material. Where usual integer derivative operators are usually limited to a relatively weak frequency bandwidth, an approach based on fractional derivatives provides good accuracy between measured hysteresis loops and simulated ones far beyond frequency bandwidth of classical piezoelectric systems. The behavior of piezo ceramics under weak electric fields excitation is usually described by constitutive relations linearized around an operating point. The ceramic comportment as the frequency is varying known as the dielectric relaxation gives important information about the piezo ceramic constitution and about the physical relations describing the polarization behavior. These characteristics are usually monitored using impedance analyzer. Dielectric relaxation is defined as the momentary delay in the dielectric constant of a material. This relaxation is usually described in terms of permittivity as a function of frequency, which can, for ideal systems, be described by the Debye complex formula [9]:

$$\varepsilon^*(\omega) = \varepsilon_\infty + \frac{\Delta\varepsilon}{1 + \mathrm{i}\omega\tau}. \tag{10.1}$$

Here ε_∞ is the sample permittivity under high-frequency excitation, $\Delta\varepsilon = \varepsilon_s - \varepsilon_\infty$ where ε_s is the quasi-static, low-frequency permittivity, and τ is the characteristic relaxation time. In the case of $BaTiO_3$ classic piezo ceramic, the Debye equation for the frequency dependence of the complex permittivity is extended to Cole-Cole model [10, 11]:

$$\varepsilon^*(\omega) = \varepsilon'(\omega) - \mathrm{i}\varepsilon''(\omega) = \varepsilon_\infty + \frac{\Delta\varepsilon}{1 + (\mathrm{i}\omega\tau)^\alpha}, \tag{10.2}$$

where $\varepsilon'(\omega)$ and $\varepsilon''(\omega)$ are the real and imaginary part of the permittivity, respectively. α is linked to the distribution of relaxation time ($0 < \alpha < 1$). Cole-Cole model gives a fractional dependence of the permittivity versus the frequency and gives correct simulation results of a piezo ceramic sample. In case of ferroelectric polymers, an extended version is proposed to consider the unsymmetrical and broadness of the dielectric dispersion curve. This extension called Havriliak-Negami [12] relaxation requires two fractional parameters:

$$\varepsilon^*(\omega) = \varepsilon'(\omega) - \mathrm{i}\varepsilon''(\omega) = \varepsilon_\infty + \frac{\Delta\varepsilon}{(1 + (\mathrm{i}\omega\tau)^\alpha)^\beta}, \tag{10.3}$$

with an additional fractional exponent β. In this article, we establish the link between the fractional operators used in the high-amplitude dielectric hysteresis model and the fractional dielectric permittivity models (Cole-Cole), well adapted to the large bandwidth frequency dependence of the permittivity. We also verify if the dynamic mechanisms responsible to the hysteresis frequency dependence are similar to those linked to the frequency dependence of the permittivity.

10.2 Nonlinear Model Using a Fractional Derivative

10.2.1 High Excitation Amplitude Fractional Hysteresis Model

The high-amplitude fractional dielectric hysteresis model is used in this study. This model has already been tested successfully previously [13, 14]. Furthermore, it is described precisely with a large number of comparisons of measure/simulation to illustrate its efficiency [15, 16]. The model is constituted of two contributions. A quasi-static contribution related to the low-frequency behavior ($f \ll 1\,\text{Hz}$) and a dynamic contribution based on fractional operators and related to the frequency dependence of the hysteresis.

10.2.1.1 Quasi-Static Contribution

The easiest way to observe the quasi-static contribution is to plot the spontaneous polarization P, versus the electric field E, at very low frequencies ($f \ll 1\,\text{Hz}$). At such frequency levels, we assume that Bloch wall movements will behave similarly to mechanical-like dry friction oscillations [13, 14]. Stressed by an external excitation, Bloch walls jump successively from one pinning defect to another until they reach a steady state where a minimum energy level is obtained. Each jump can be considered as a small mechanical dry friction, and consequently as a small amount of losses. A static (frequency-independent) equation based on its mechanical dry-friction counterpart has been established in order to consider this property. Basically, this equation describes how a major symmetrical hysteresis loop $P(E)$ can be obtained by translating a hysteretic curve. The sign of the translation is equal to the sign of the time derivative of the polarization and the amplitude equal to the coercive field, Ec. In the time domain, the polarization can be written as:

$$P(t) = F\left(E(t) - E_c \text{sgn}\left(\frac{\text{d}P(t)}{\text{d}t}\right)\right). \tag{10.4}$$

Here, $F(E)$ (or inversely $F^{-1}(P)$) represents the behavior of a nonlinear dielectric. Its mathematical description is as follows:

$$F(E(t)) = \sigma \tan^{-1}\left(\frac{E(t)}{\gamma}\right). \tag{10.5}$$

An experimental protocol has been defined to obtain this $F(.)$ function. This procedure details are explained in detail in [13]. The parameters γ, σ and the function F are obtained by fitting the tested samples' experimental anhysteretic curve to the analytical expression (Eq. 10.5). Unfortunately, due to its simplicity, Eq. 10.4 is limited to the description of symmetrical major hysteresis loops observed during steady state and for high-amplitude electrical field ($E_0 \gg E_c$). Differences with experimental results will appear as soon as the excitation is no longer symmetrical (first polarization curve, minor hysteresis loops). Equation 10.4 is limited to just a single Bloch wall movement. To overcome this limitation and to get an accurate model independent of the experimental situation, we need to take into account a large number of domain wall dry frictions, as is the case experimentally. A distribution of mechanical dry frictions (called spectrum), characterized by their own coercive fields E_{ci} and polarization P_i in addition to their own weights, is taken into account to converge into much more precise simulation result:

$$P_i = F\left(E(t) - E_{ci}\,\mathrm{sgn}\left(\frac{\mathrm{d}P_i(t)}{\mathrm{d}t}\right)\right), \tag{10.6}$$

$$\sum_{i=1}^{k} \mathrm{Spectrum}(i) \times P_i(t) = P(t). \tag{10.7}$$

Spectrum(i) represents the distribution of these basic dry frictions (wall movements). A deconvolution between the experimental first polarization curve and the F function allows to obtain this distribution. Large number of results as well as further information concerning the static model are available in [13–17].

10.2.1.2 Dynamic Contribution

Usually, frequency dependence in ferroelectric hysteresis models (Eqs. 10.6, 10.7) is considered by adding a viscous losses term to the quasi-static contribution. Such a consideration modifies Eq. 10.4 in the following way:

$$P(t) = F\left(E(t) - E_c\,\mathrm{sgn}\left(\frac{\mathrm{d}P(t)}{\mathrm{d}t} + \rho\frac{\mathrm{d}P(t)}{\mathrm{d}t}\right)\right). \tag{10.8}$$

Unfortunately, simple experimental test quickly demonstrates that this equation can only be used with a moderate accuracy on a restrained frequency bandwidth. If the comparison of simulation/measure for the *amplitude-versus-frequency* curve correctly fits the low-frequency range, the difference for the increasing frequency is important. The viscous losses term $\rho \mathrm{d}P/\mathrm{d}t$, where ρ is a material constant, in Eq. 10.8 leads to an overestimation of the high-frequency component of the polarization signal. To overcome this problem, we need an operator that balances the low-frequency and the high-frequency component in a different way than a straight time derivative. Such operators exist in the framework of fractional calculus;

there are so-called non-entire derivatives or fractional derivatives. The fractional derivative generalizes the concept of derivative to non-integer orders. The fractional derivative of a smooth (arbitrary) function $g(t)$ is defined through a convolution between $g(t)$ function and $t^{\alpha}\Theta(t)/\,\Gamma(1-\alpha)$ where $\Gamma(\alpha)$ is the gamma function; α, the order of fractional derivation; and $\Theta(t)$ is the step Heaviside function (see [12], while a summary of various representations can be found in [18]). After addition of fractional terms in our simulation, the model equations (Eqs. 10.6, 10.7) become:

$$P_i = F\left(E(t) - E_{ci}\,\mathrm{sgn}\left(\frac{\mathrm{d}P_i(t)}{\mathrm{d}t} + \rho\frac{\mathrm{d}^{\alpha}P_i(t)}{\mathrm{d}t^{\alpha}}\right)\right), \tag{10.9}$$

$$\sum_{i=1}^{k}\mathrm{Spectrum}(i)\times P_i(t) = P(t). \tag{10.10}$$

10.2.2 Model for the Complex Permittivity Under Weak Electric Field

At room temperature and as the electric field is weak, we admit that the real part $\varepsilon(\omega)$ and the imaginary part $\varepsilon(\omega)$ of the complex permittivity measured around an operating point are just frequency dependent. Both components of the complex dielectric permittivity are linked to each other by the well-known Kramers-Kronig relations [17]. Debyes model has been one of the first models proposed to deal with the dielectric relaxation. But first experimental results have rapidly shown that corrections of that simple model will be necessary for a correct description. The Cole-Coles model introduces an improvement considering a distribution function for the relaxation time. This correction has been possible as a result of the extension of the Debyes model to a non-entire order. Cole-Coles model is indeed a frequency fractional dependence of the evolution of the complex permittivity. From the Cole-Coles model, $\varepsilon(\omega)$ and $\varepsilon(\omega)$ can be written as:

$$\varepsilon'(\omega) = \varepsilon_{\infty} + \frac{\Delta\varepsilon'}{2}\left\{1 - \frac{\sinh(\beta z)}{\cosh(\beta z) + \cos\left(\beta\frac{\pi}{2}\right)}\right. \quad , \tag{10.11}$$

$$\varepsilon''(\omega) = \frac{\Delta\varepsilon'}{2}\left\{1 - \frac{\sinh(\beta\frac{\pi}{2})}{\cosh(\beta z) + \cos\left(\beta\frac{\pi}{2}\right)}\right. \quad , \tag{10.12}$$

In the above expressions $z = \ln(\omega\tau)$, $\Delta\varepsilon = \varepsilon_s - \varepsilon_{\infty}$, and $\beta = (1-\alpha)$, where α shows the deformation of the semicircle arc in the Cole-Cole plot, i.e., it is the angle from the ε axis to the center of the semicircle arc. $\varepsilon(\omega)$ is related to the stored energy within the sample. $\varepsilon(\omega)$ is related to the dissipation (loss) of energy within the medium. According to the Cole-Coles model, the complex permittivity ε^* may be written as:

$$\varepsilon^* = \varepsilon'(\omega) - \mathrm{i}\varepsilon''(\omega) = \varepsilon_\infty + \frac{\Delta\varepsilon}{1 + (\mathrm{i}\omega\tau)^\alpha} \tag{10.13}$$

with $\Delta\varepsilon = \varepsilon_s - \varepsilon_\infty$ and $0 < \alpha = 1 - 2\sigma/\pi \leq 1$, while σ is the angle with respect to the semicircle center. Various methods can be employed to determine this angle [18].

10.2.3 Relation Between High Excitation Amplitude Dielectric Hysteresis Fractional Model and the Complex Permittivity Cole-Cole Model

We start with a weak excitation contribution, sufficiently weak to assume that even for hysteretic material cases, there are linear relations between the dielectric polarization P and the electric field E. If the frequency is small and the polarization is harmonic:

$$P(t) = P_0 \cos(\omega t) \tag{10.14}$$

the static (instantaneous) contribution of E is given by:

$$E_{\mathrm{stat}}(t) = \frac{P_0 \cos(\omega t)}{\varepsilon_{\mathrm{stat}}} \tag{10.15}$$

As the frequency is increasing, the dynamic contribution of the electric field is considered because of the fractional relation as it is the case in the hysteresis fractional model:

$$E_{\mathrm{dyn}}(t) = \rho \frac{\mathrm{d}^\alpha P}{\mathrm{d}t^\alpha}. \tag{10.16}$$

Here P is a harmonic-type waveform, so the dynamic contribution of the electric field can be expressed by its analytical solution:

$$E_{\mathrm{dyn}}(t) = \rho P_0 \omega^\alpha \cos\left(\omega t + \alpha \frac{\pi}{2}\right). \tag{10.17}$$

Finally, for higher frequencies, the electrical field including all contributions is described by:

$$E(t) = \rho P_0 \omega^\alpha \cos\left(\omega t + \alpha \frac{\pi}{2}\right) + \frac{P_0 \cos(\omega t)}{\varepsilon_{\mathrm{stat}}} \tag{10.18}$$

In the complex representation, an electric field $\Re\{\underline{E}(t)\} = E(t)$ and a corresponding dielectric coefficient $\underline{\varepsilon}$ can be written as follows:

$$\underline{E}(t) = P_0 \exp(\mathrm{i}\omega t)\left[\frac{1}{\varepsilon_{\text{stat}}} + \rho\omega^{\alpha}\exp\left(\mathrm{i}\alpha\frac{\pi}{2}\right)\right], \tag{10.19}$$

$$\underline{\varepsilon} = \frac{1}{\dfrac{1}{\varepsilon_{\text{stat}}} + \rho\omega^{\alpha}\mathrm{e}^{\mathrm{i}\alpha\dfrac{\pi}{2}}}, \tag{10.20}$$

$$\underline{\varepsilon} = \frac{\varepsilon_{\text{stat}}}{1 + \varepsilon_{\text{stat}}\rho\omega^{\alpha}\mathrm{i}^{\alpha}}. \tag{10.21}$$

Finally,

$$\underline{\varepsilon} = \frac{\varepsilon_{\text{stat}}}{1 + (\mathrm{i}\omega\tau)^{\alpha}}, \quad \text{where} \quad \tau^{\alpha} = \rho\varepsilon_{\text{stat}}. \tag{10.22}$$

If we assume $\varepsilon(0) \gg \varepsilon_{\infty}$ which is obviously our case as we work with piezoceramic where $\varepsilon(0) \approx 1800$ and $\varepsilon_{\infty} \approx 100$, the relation between Cole-Coles model and our high electric field amplitude model is clear:

$$\underline{\varepsilon} = \varepsilon_{\infty} + \frac{\varepsilon(0) - \varepsilon_{\infty}}{1 + (\mathrm{i}\omega\tau)^{\alpha)}} \approx \frac{\varepsilon_{\text{stat}}}{1 + (\mathrm{i}\omega\tau)^{\alpha)}}. \tag{10.23}$$

10.3 Characterization and Experimental Validation

A soft PZT composition (P188 obtained from Quartz & Silice, France, Navy type II) has been tested in this study (Table 10.1).

Cylindrical specimens (of 6.35 mm diameter and 4 mm height) are exposed to the external electric field. Constant temperature conditions and free mechanical properties of the sample are assumed.

10.3.1 High-Amplitude Electric Field Characterization

The excitation electric field is dimensioned to provide a maximal value close to 2 kV/mm. Under such level of excitation, we highly exceed the coercive field of the

Table 10.1 PZT (P188) material parameters

Parameter	Symbol	Units	Typical value
Density	ρ'	10^3 kg m^{-3}	7.7
Poisson's constant	σ'	–	0.3
Curie temperature	T_c	°C	340
Dielectric permittivity	$\varepsilon_{33}^{T}/\varepsilon_0$	–	1850
Piezoelectric coefficient	d_{33}	pC/N	425

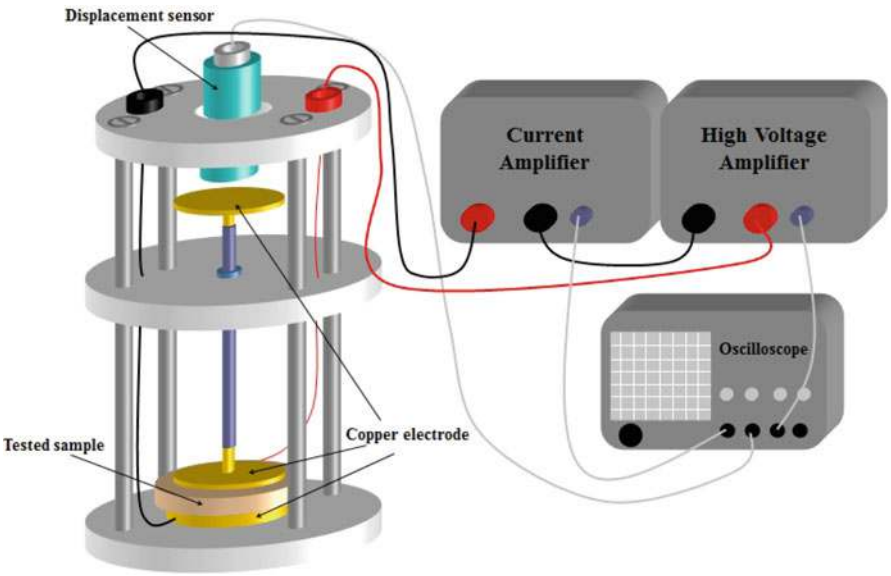

Fig. 10.1 Experimental measuring setup

material. A sinus signal of controlled frequency is used as input of a 10 kV Optilas Trek high-voltage amplifier. To avoid dielectric breakdown, the specimens are electrically insulated with silicon grease. The electric current is monitored by charge measurement (Kistler amplifier 5011). The polarization field is determined by integration of the charge measurement. Post processing, the numerical integration is performed. Figure 10.1 presents the experimental measuring setup especially developed for the high-amplitude electric field characterization. The role of the rod in the middle of the frame is to transmit the tested samples displacement to the displacement sensor. Even if the rod can have side effect because of its inertia, we have checked using laser vibrometer that the mechanical displacements are correctly transmitted by the system. For an electric field amplitude close to 2 kV, the frequency limitation of the high-voltage amplifier is close to 100 Hz for ceramics of 6 mm diameter.

The excitation signal provided by the impedance analyzer consists of an AC sine of varying frequency with a maximal value corresponding to 1 V. The analyzer behaves as a perfect voltage source. The electrical current crossing the tested sample is monitored simultaneously. From the imposed voltage and from the measured current, the impedance analyzer provides instantaneously the paralleled voltage-equivalent capacitance and the losses angle versus the frequency. The analyzer generates a linear sweep on a large frequency bandwidth available (40 Hz–40 MHz). In this study the maximum frequency tested has been reduced to 50 kHz to avoid the mechanical resonances which completely disturb the measure.

10.4 Experimental Results

Among others, an objective of this study is to check the accuracy of the fractional operators taken into account and the frequency dependence of the dielectric losses in a ferroelectric material. Both situations were tested then, the complex dielectric permittivity and the dielectric hysteresis dynamic under high level of external electric field.

As illustrated, in the model description in the above section, a theoretical frequency dependence relation can be established between Cole-Cole dielectric permittivity model and high excitation amplitude hysteresis model. In this experimental part, comparison of simulation/measure is exposed to validate first the viability of our theory and to check next if the dynamic parameters can be conserved through the scales. If this statement is confirmed, it means that whatever the scale, the dynamical behaviors are similar. It confirms too that a simple impedance meter analysis is enough to parameterize the materials ferroelectric dynamic behavior. Figure 10.2 shows comparisons of simulation/measure obtained under quasi-static conditions.

Figure 10.3 shows the quasi-static, high excitation amplitude, model parameters. Figure 10.4 shows similar comparisons for frequency varying from 2 MHz to 50 Hz. It is worth noticing that Fig. 10.4 exhibits good simulation/measure correlations on high-amplitude hysteresis loops. Unfortunately on such kind of measures, the high-frequency limit is rapidly reached. Beyond this maximal frequency, the current required to polarize the piezo ceramic is so high that the voltage amplifier is no longer suitable to provide it. One solution is to reduce the surface area of the tested sample, but even with a maximal reduction, we are rapidly limited. For better clarity, Fig. 10.5 illustrates the limitation of the first-order derivative model. In this figure, we have intentionally plotted only the high-frequency simulation results obtained for $\alpha = 0.53$. However, the results obtained for $f = 0.5\,\text{Hz}$ and higher are similar to those obtained as $\alpha = 1$. After validation of the high-amplitude excitation dynamic hysteresis model, it is time now to focus on complex dielectric model. Impedance meter gives the frequency evolution of the real and the imaginary part of the permittivity.

Cole-Cole plot can be obtained then and compared to those obtained with the Cole-Cole model. Cole-Cole model is configured using the same parameters to those giving good results with the hysteresis model. Unfortunately, the high-frequency limit of the impedance meter is relatively low. Indeed, as soon as the first mechanical resonant appears, the impedance of the tested sample changes radically, and the voltage source is no longer suitable to supply to the ceramic. The half circle Cole-Cole plot obtained is actually not even one third of a circle. The frequency bandwidth tested is sufficiently large to conclude that the comparisons obtained give very interesting results. The simulated curves obtained with the Cole-Cole model and the experimental ones fit almost perfectly and validate our expectations. The physical behaviors responsible for the dynamic dielectric losses are similar under

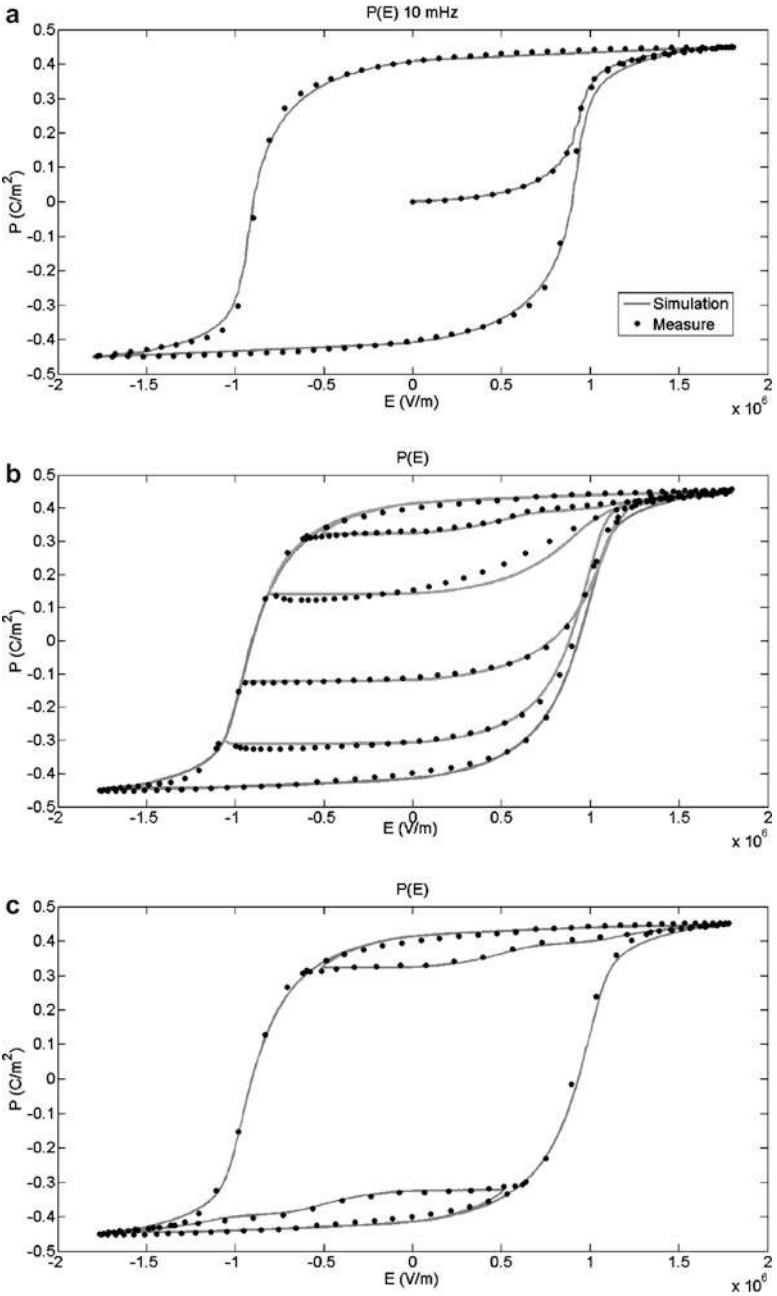

Fig. 10.2 Comparison of simulation and measurement results in a quasi-static limit ($f < 50$ mHz) for different initial polarizations (initial conditions for (**a**)–(**c**))

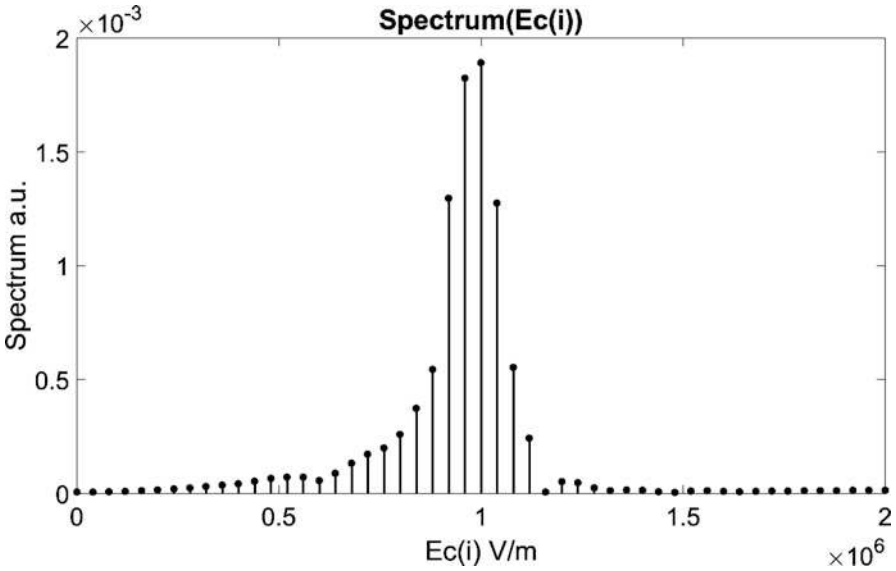

Fig. 10.3 Spectrum distribution function and model parameters fitted to the experiment. The system parameters are presented in Table 10.2

Table 10.2 Simulation parameters

Quasistatic parameters		Dynamic parameters	
Symbol	Value	Symbol	Value
γ	1000	α 0.53	
σ	30	ρ	50,000

high and weak electrical excitation field. They can then be modelled using the same operators. This observation is particularly interesting because it allows limiting the piezo ceramic characterization to the impedance analyzer (where all the dynamic model parameters can be set) and to anticipate the high electrical amplitude stress behavior in simulation. Impedance analyzer measures are quick and easy and can be repeated without special attention which is obviously not the case in high-amplitude hysteresis measure.

10.5 Conclusions

Fractional operators taken into account the dynamic dielectric losses through a piezo ceramic material under high electrical excitation were tested successfully in the past [14, 19–21]. This technique gives good accuracy on frequency dependence of hysteresis loops (see full black lines with $\alpha \approx 0.5$ in Fig. 10.4). It also allows to

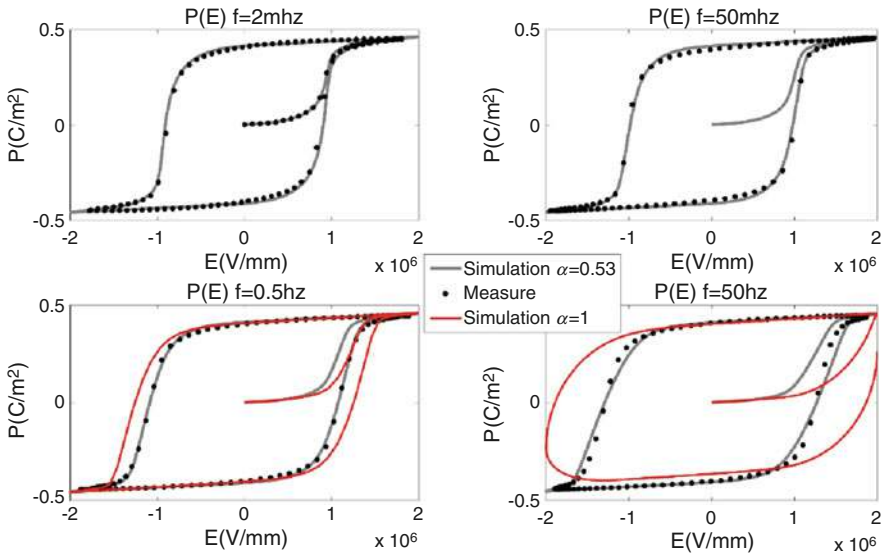

Fig. 10.4 Comparison of simulation and measurement results under dynamic conditions. Note that the convergence of the simulated (black line) for $\alpha \approx 0.5$ and experimental results (black points) and the lack of convergence (simulation results in red lines lower panels) for $\alpha = 1$

envisage other dynamic manifestations such as creep behavior, ageing, and extended electrode contacts. In this article, the link between the fractional consideration used under high electric field amplitude in the limit of low frequency (required for hysteresis loop plots) and very low excitation level but high-frequency bandwidth measures was obtained using an impedance analyzer and discussed in the context of the Cole-Cole model. In both limits, it was confirmed that the dynamic losses exhibit the same physical origin, and consequently they could be modelled using the same operators and the same parameters. This notation is particularly interesting because it allows to reduce the piezo ceramic characterization to the impedance analyzer characterization. In this article, authors have focused their study to soft piezo ceramics. Future work will deal with other types of ferroelectric material such as polymers.

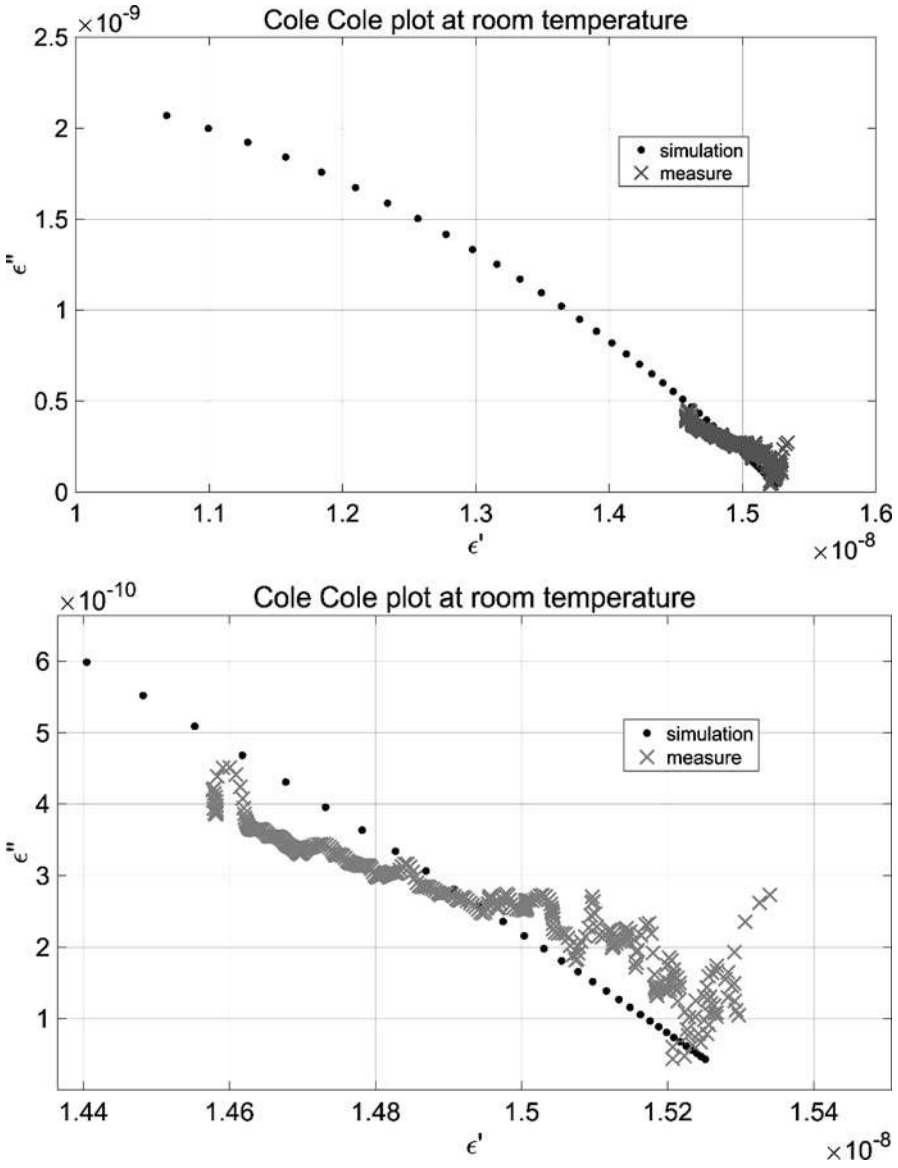

Fig. 10.5 Comparison of simulation and measurement results in the Cole-Cole plot ($\varepsilon(\omega)$ versus ($\varepsilon(\omega)$)

Acknowledgements The authors would like to thank for the support from the Polish-French collaboration project (Polonium).

References

1. Cillesen, J.F.M., Giesbers, J.B., Weening, R.P., Wolf, R.M.: A ferroelectric transparent thin-film transistor. Appl. Phys. Lett. **68**, 3650–3652, (1996)
2. Prins, M.W.J., Zinnemers, S.E., Cillessen, J.F.M., Giesberg, J.B.: Depletion-type thin-film transistors with a ferroelectric insulator. Appl. Phys. Lett. **70**, 458–460 (1997)
3. Yong, T.K., Dong, S.S.: Memory window of Pt/SrBi2Ta2O9/CeO2/SiO2/Si structure for metal ferroelectric insulator. Appl. Phys. Lett. **71**, 3507–3509 (1997)
4. Boser, 0.: Statistical theory of hysteresis in ferroelectric materials. J. Appl. Phys. **62**, 1344–1348 (1987)
5. Morita, T., Ishii, Y., Fukai, I.: Hysteresis model using distribution susceptibility. J. Appl. Phys. **73**, 7025–7029 (1993)
6. Potter, B.G. Jr., Tikare, V., Tuttle, B.A.: Monte carlo simulation of ferroelectric phase transition. J. Appl. Phys. **87**, 4415–4424 (2000)
7. Bartic, A.T., Wouters, D.J., Maes, H.E., Rickes, J.T., Waser, R.M.: Preisach model for the simulation of ferroelectric capacitors. J. Appl. Phys. **89**, 3420–3425 (2001)
8. Sivasubramanian, S., Widom, A., Strivastava, Y.: Equivalent circuit and simulations for the Landau-Khalatniko model of ferroelectric hysteresis. IEEE Trans. Ultras. Ferro. Freq. Cont. **50**, 950–957 (2003)
9. Debye, P.: Zur Theorie der anomalen dispersion im Gebiete der langwelligen Elektrischen Strahlung. Ver. Deut. Phys. Gesell. **15** 777–793 (1913)
10. Cole, K.S., Cole, R.H.: Dispersion and absorption in dielectrics – I alternating current characteristics. J. Chem. Phys. **9** 341–352, (1941)
11. Cole, K.S., Cole, R.H.: Dispersion and absorption in dielectrics – II direct current characteristics. J. Chem. Phys. **10**, 98–105 (1942)
12. Havriliak, S., Negami, S.: A complex plane representation of dielectric and mechanical relaxation processes in some polymers. Polymer **8**, 161–210 (1967)
13. Ducharne, B., Guyomar, D., Sebald, G.: Low frequency modelling of hysteresis behaviour and dielectric permittivity in ferroelectric ceramics under electric field. J. Phys. D: Appl. Phys. **40**, 551–555 (2007)
14. Guyomar, D., Ducharne, B., Sebald, G.: Time fractional derivatives for voltage creep in ferroelectric materials: theory and experiment. J. Phys. D: Appl. Phys. **41**, 125410 (2008)
15. Zhang, B., Ducharne, B., Guyomar, D., Sebald, G.: Energy harvesting based on piezoelectric Ericsson cycles in a piezo ceramic material. Eur. Phys. J. S.T. **222**, 1733–1743 (2013)
16. Guyomar, D., Ducharne, B., Sebald, G.: High frequency bandwidth polarization and strain control using a fractional derivative inverse model. Smart Mater. Struct. **19**, 045010 (2010)
17. Rouleau, L., Deu, J.F., Legay, A., Le Lay, F.: Application of Kramers-Kronig relations to time-temperature superposition for viscoelastic materials. Mech. Mater. **65**, 66–75 (2013)
18. Nguyen, D.Q., Lebey, T., Castelan, P., Bley, V., Boulos, M., Guillemet-Fritsch, S., Combetten, C., Durand, B.: Electrical and physical characterization of bulk ceramics and thick layers of barium titanate manufactured using nanopowders. J. Mat. Eng. Perf. **16**, 626–634 (2007)
19. Weron, K., Klauzer, A.: Probabilistic basis for the Cole-Cole relaxation law. Fermelecrrics **236**, 59–69 (2000)
20. Rekanos, I.T., Yioultsis, T.V.: Approximation of GrünwaldLetnikov fractional derivative for FDTD modeling of Cole-Cole media. IEEE Trans. Magn. **50**, 7004304 (2014)
21. Lewandowski, M., Orzylowski, M.: Fractional-order models: the case study of the supercapacitor capacitance measurement. Bull. Pol. Acad. Sci. Chem. **65**, 449–457 (2017)